Research Article Vol. 29, No. 6 / 15 March 2021 / Optics Express 8606
Optics EXPRESS

Orders of magnitude loss reduction in photonic bandgap fibers by engineering the core surround

S. UPENDAR,[1] R. F. ANDO,[2] M. A. SCHMIDT,[2,3] AND T. WEISS[1,*]

[1] 4th Physics Institute and Research Center SCoPE, University of Stuttgart, Pfaffenwaldring 57, 70569 Stuttgart, Germany
[2] Leibniz Institute of Photonic Technology, e.V. Albert-Einstein-Str. 9, 07745 Jena, Germany
[3] Otto Schott Institute of Material Research, Friedrich Schiller University, Fraunhoferstr. 6, 07743 Jena, Germany
[*] t.weiss@pi4.uni-stuttgart.de

Abstract: We demonstrate how to reduce the loss in photonic bandgap fibers by orders of magnitude by varying the radius of the corner strands in the core surround. As a fundamental working principle we find that changing the corner strand radius can lead to backscattering of light into the fiber core. Selecting an optimal corner strand radius can thus reduce the loss of the fundamental core mode in a specific wavelength range by almost two orders of magnitude when compared to an unmodified cladding structure. Using the optimal corner radius for each transmission window, we observe the low-loss behavior for the first and second bandgaps, with the losses in the second bandgap being even lower than that of the first one. Our approach of reducing the confinement loss is conceptually applicable to all kinds of photonic bandgap fibers including hollow core and all-glass fibers as well as on-chip light cages. Therefore, our concept paves the way to low-loss light guidance in such systems with substantially reduced fabrication complexity.

1. Introduction

In photonic bandgap fibers, light is guided inside a central defect core of an otherwise perfectly periodic lattice, yielding a photonic bandgap along the fiber axis at certain wavelength ranges [1]. Light guidance can take place in a core with a lower index than the average index of the periodic cladding, enabling a large number of applications that cannot be accessed in conventional optical fibers. Examples are sensing in liquid-filled cores [2,3], nonlinear effects in gas-filled cores [4,5], broad tunability for supercontinuum generation [6], and many other applications [7–10]. Recently, the idea of photonic bandgap guidance in hollow waveguides with cylindrical inclusions has also transferred to planar waveguide technology on the basis of the light cages concept implemented by 3D nanoprinting [11,12]. It turns out that the losses of fabricated bandgap fibers are higher than in conventional step-index fibers due to the following reasons: First, the periodic lattice consists of a finite number of rings of high-index inclusions, thus light can leak through the microstructured region to the homogeneous surrounding of the fiber. This confinement loss can be in principle decreased by increasing the number of rings of high-index inclusions. In practice, this yields a significantly increased effort for fabricating such fibers. Second, large deviations from the ideal design due to fabrication inaccuracies can lead to high losses. Third, the guided light can be scattered at imperfections along the direction of propagation, particularly within the first cladding ring, which is on the order of 1 dB/km [13]. One reason for this scattering loss are frozen-in capillary waves that occur during the fabrication process [13,14]. Another key factor for increased attenuation in low-index-contrast bandgap fibers can be bend loss [15]. In this work,

#416030 https://doi.org/10.1364/OE.416030
Journal © 2021 Received 27 Nov 2020; revised 29 Jan 2021; accepted 29 Jan 2021; published 4 Mar 2021

Optics EXPRESS

we focus on providing design rules for minimizing confinement loss on the basis of structural modifications.

A large number of theoretical and experimental studies has been devoted to tailoring the properties and reducing the losses of photonic bandgap fibers by introducing structural changes in the cladding and core surround, e.g., by adding index depressed layers in the unit cell [16,17], selective index or radius variations of specific inclusions in the cladding [18–21], introducing additional structures in the core [22–24] or removing inclusions in the vicinity of the core [25]. It is well known that structural changes near the core affects the propagation of the fundamental core mode most significantly [26]. Particularly, so-called surface modes in hollow core photonic bandgap fibers and cladding supermodes in high-index inclusion bandgap fibers [24,27,28] reduce the bandwidth and increase the losses of the fiber [29].

Here, we introduce the concept of corner strand modification by changing the corner strand radius in a photonic bandgap fiber with higher-index strands. This yields an optimal radius of these corner strands, for which the losses of the fundamental mode can be orders of magnitude lower than in the unmodified cladding structure. We also compare our results with the case of missing corner strands described in Ref. [25] for the first and second bandgap. We find that for certain ratios of strand radius r and pitch Λ, the removal and size modification of corner strands lead to a comparable reduction of loss within the first bandgap. However, the missing corner strands fail to reduce losses for higher-order bandgaps and also for particular ranges of the ratio r/Λ in the first bandgap. In order to analyze this phenomenon, we carry out a parameter study and a quantitative comparison of the different mode profiles, which has been achieved by normalizing the fiber modes using the procedure described in Refs. [30,31]. As in the case of missing corner strands, the loss reduction mainly arises from the backscattering of light to the fiber core due to the presence of the modified inclusions. We also show that this low loss behavior is tolerant towards fabricational imperfections such as position and diameter deviations.

2. Results and discussion

As a test system, we consider a photonic bandgap fiber that includes high-refractive-index cylindrical inclusions made of $n_{\mathrm{high}} = 1.59$ (coresponding to CS_2 [32]) arranged in a triangular lattice and embedded into a homogenous background of $n_{\mathrm{low}} = 1.44$ (corresponding to silica [33]). We define the center-to-center interstrand distance as pitch Λ with the ratio $r/\Lambda = 0.2$ with $r = 0.764$ µm. The corner strand radius R differs from the radius r of the otherwise perfect cladding structure [see Fig. 1 bottom panel schematic]. The structural parameters of the test fiber system are chosen such that we obtain a loss minimum, by modifying the corner strands, at a wavelength of 1.55 µm. The considered fiber geometry comprises four cladding rings with seven missing inclusions in the center acting as the defect core. A schematic of the proposed structure with modified corner strands can be seen in Fig. 1 at the bottom right of (b), while the schematics referring to Fig. 1(a) denote conventional unmodified fiber structures with $R = r$.

The modes propagating in such systems are eigensolutions of Maxwell's equations with outgoing boundary conditions in the absence of sources. The eigenvalues are complex-valued propagation constants $\beta = k_0 n_{\mathrm{eff}}$, with k_0 and n_{eff} being the free-space wave vector and the effective refractive index respectively, and the imaginary part of n_{eff} denoting the modal attenuation. Here, the eigensolutions are calculated using the multipole expansion method [34,35].

We first analyze the modal attenuation for different radii of inclusion for unmodified corner strands with radius $R = r$. In Fig. 1(a), we plot the loss as a function of V parameter, which is defined as

$$V = \frac{2\pi r\sqrt{n_{\mathrm{high}}^2 - n_{\mathrm{low}}^2}}{\lambda}. \tag{1}$$

Optics EXPRESS

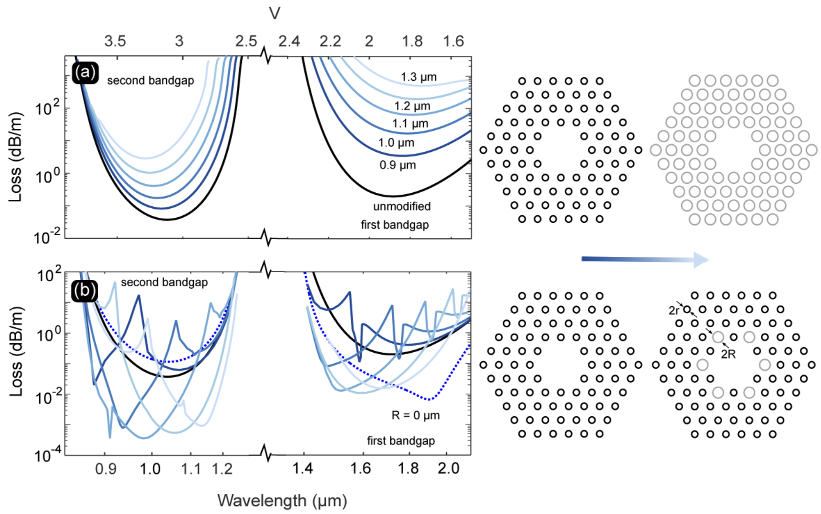

Fig. 1. (a) Loss as a function of V parameter for varying strand radius r for the first and second bandgap. Schematics of the structures with increasing strand radius are shown on the top right, for a constant pitch of $\Lambda = 3.82$ µm. Panel (b) displays the loss for different corner strand radii R for the first and second bandgap. The strand radius of the unmodified structure is $r = 0.764$ µm. The colors denote different radii of inclusion in the cladding in (a), while they indicate different corner strand radii in (b), ranging between 0.9 µm and 1.3 µm [see labels in (a)]. A schematic along with its modified version with enlarged corner strands (gray circles) in the core surround is shown on the bottom right. Comparison of panels (a) and (b), with the scale of loss being two orders of magnitude lower in (b), reveals that the optimal structure with the lowest loss is obtained in the first and second bandgap for missing (blue dotted line) and modified corner strands (blue solid lines), respectively. In the case of the latter, the corner strand radius of minimum loss is $R = 0.27$ µm. Note that the V parameter axis is related to the radius of inclusions outside the first cladding ring and holds for top and bottom panels, while the wavelength axis corresponds only to the results in the bottom panel, where the radius of the cladding strands is fixed to $r = 0.764$ µm.

Schematics of the different fiber structures are shown in Fig. 1 to the right. Interestingly, the loss in the second bandgap is lower than that of the first bandgap even for the unmodified cladding structure, which has already been observed for other fibers with low index contrast between the high-index inclusions and low-index background [36]. Figure 1(b) provides the confinement loss for the fundamental mode (i.e., the mode with the largest magnitude of the electric field at the center of the core) for different corner strand radii R as a function of wavelength across the first and second bandgap. For the first bandgap, it is seen that while enlarging the corner strand radius does reduce the losses by almost two orders of magnitude compared to the fiber with the conventional unmodified cladding, the geometry with missing corner strands gives the lowest loss. In contrast, for the second bandgap, we observe that the optimal structure for lowest loss is with modified corner strand radius, see Fig. 1(b).

We now compare the dispersion of the effective index of the fundamental core mode for the cladding structures with $R = r$, $R \approx 1.5r$, and $R = 0$ for the first bandgap. The real and imaginary part of the effective index are plotted in Fig. 2(a) and (b), respectively. The unmodified and missing-corner-strand structures show a smooth evolution for both the real and imaginary part (denoted by black solid lines and red dashed lines, respectively) across the bandgap with high $\mathrm{Im}(n_{\mathrm{eff}})$ at the band edges due to the presence of a large number of cladding states, and a minimum at the center of the bandgap. The effective index for the structure with enlarged corner strands

(R = 1.16 μm), corresponding to the radius providing the lowest loss, is plotted in the same figure with blue dashed-dotted lines. It is seen that there are three distinct dispersion curves of the fundamental mode and its anticrossing with cladding supermodes.

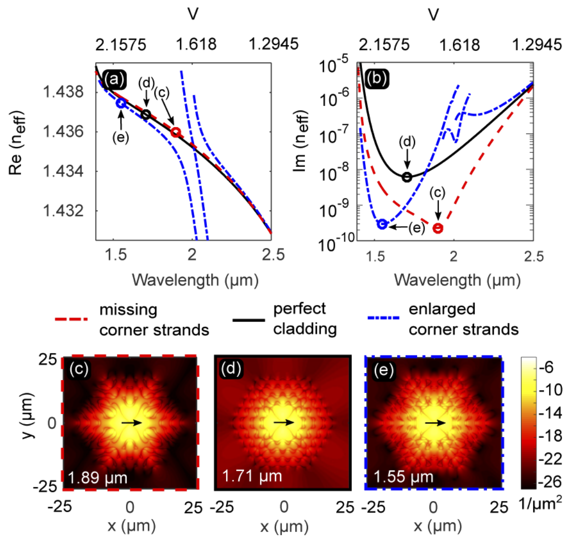

Fig. 2. Real (a) and imaginary (b) part of the effective index of the fundamental core mode and its possible anticrossings with cladding supermodes with (blue dashed-dotted lines) and without (black solid lines) modified as well as missing (red dashed lines) corner strands in the core surround for the first bandgap. The pitch is Λ = 3.82 μm, the strand radius is r = 0.764 μm, and the modified corner strand radius is R = 1.16 μm, which corresponds to the lowest loss structure when enlarging the corner strands. The normalized absolute value S_ρ in logarithmic scale (c-d) is plotted for x-polarized modes at the wavelength of lowest loss for structures with missing (c), conventional (d), and optimized (e) corner strands. The field distributions have been normalized analytically according to Eq. (2), so that the comparison of the magnitudes becomes physically meaningful. The best confinement is observed for the structure with missing corner strands.

We observe that between the bandgap edge and the anticrossing with the cladding supermode, Im(n_{eff}) of the fundamental core mode is almost two orders of magnitude lower for the enlarged corner strands than in the unmodified cladding structure and comparable with the loss in the missing-corner-strand structure. The loss at wavelengths close to the avoided crossing with the cladding supermodes is very high due to the leaky nature of the cladding supermodes.

The absolute value of the ρ component of the Poynting vector for missing, unmodified and enlarged corner strand (R = 1.16 μm) is shown in Fig. 2(c)-(e), respectively, at the wavelength of minimum loss for each structure. To facilitate a quantitative comparison of the Poynting vector fields, we have normalized the fields of the leaky core modes by satisfying the normalization condition [30,31]

$$S + L = 1, \tag{2}$$

where the surface term S and the line term L yield

$$S = \int_0^{2\pi} \int_0^{r_n} \rho (E_\rho H_\phi - E_\phi H_\rho) d\rho d\phi, \tag{3}$$

$$L = \frac{\varepsilon\mu k_0^2 + \beta^2}{2(\varepsilon\mu k_0^2 - \beta^2)^2} \int_0^{2\pi} \left(E_z \frac{\partial H_z}{\partial \phi} - H_z \frac{\partial E_z}{\partial \phi} \right)_{\rho=r_n} d\phi$$
$$+ \frac{k_0 \beta r_n^2}{2(\varepsilon\mu k_0^2 - \beta^2)^2} \int_0^{2\pi} \left\{ \mu \left[\left(\frac{\partial H_z}{\partial \rho} \right)^2 - \rho H_z \frac{\partial}{\partial \rho} \left(\frac{1}{\rho} \frac{\partial H_z}{\partial \rho} \right) \right] \right. \tag{4}$$
$$\left. + \varepsilon \left[\left(\frac{\partial E_z}{\partial \rho} \right)^2 - \rho E_z \frac{\partial}{\partial \rho} \left(\frac{1}{\rho} \frac{\partial E_z}{\partial \rho} \right) \right] \right\}_{\rho=r_n} d\phi.$$

Here, r_n is the radius of normalization, which spans over the regions of spatial inhomogeneities, β is the propagation constant, k_0 is the wavenumber, and ε and μ are the permittivity and permeability in the outermost cladding region. The electric and magnetic fields are denoted by E and H, respectively. It should be noted that because of the normalization, the unit of the fields is 1/µm. Equations (2) to (4) have been derived in Ref. [30] and provide the correct weight of bound and leaky fiber modes for the modal expansion of the Green's dyadic of Maxwell's equations. Based on the correct normalization, we have shown how to predict the guiding properties under structural perturbations and how to redefine the Kerr nonlinearity parameter for leaky modes [30,31,37]. Here, this normalization allows for quantitatively comparing the leakage of energy for different fiber geometries.

It can be seen in the Fig. 2(d), for the unmodified cladding, that – while most of the energy is concentrated at the central core defect – a significant portion also leaks out to the exterior silica background outside the periodic cladding. Comparing the S_ρ component for the lower loss structures of missing and modified inclusions with the unmodified cladding in panel (c) and (e), we can see that the leakage to the exterior silica background has drastically reduced for both these cases, with the missing corner strands having a slightly better confinement.

We also compare the real and imaginary parts of the effective index for the second bandgap in Fig. 3(a) and (b) for the three structures of $R = r$, $R \approx 0.35r$ and $R \approx 1.45r$. The structure with missing corner strands is not considered for the second bandgap, as it turns out that such geometry does not reduce the losses. The unmodified cladding and the structure with reduced corner strands have a smooth dispersion for the real and imaginary part. Taking a look at the structure with enlarged corner strands of $R = 1.11$ µm, we can see that there are four distinct curves for the fundamental mode and its anticrossings with the cladding supermodes, due to the presence of a higher number of cladding supermodes in the second bandgap. We can see in Fig. 3(b) that the low loss behavior is exihibited by both the structures with modified corner strands. Looking at the S_ρ component at the wavelength of minimum loss, we can see that the leakage to the exterior silica background is very high for the unmodified cladding (d) photonic bandgap fiber. In contrast, a huge reduction of leakage to the exterior background is clearly visible for the proposed structures of modified corner strands (c) and (e). This implies that there is a redistribution of energy density due to the presence of the modified corner strands, which is the reason for the low loss behavior observed in the spectral distribution of the loss in the proposed structures. Hence, the variation of the radius of corner strands in the core surround represents a new way to achieve lower loss values without adding any additional rings to the cladding structure for both bandgaps. Therefore, we expect that such a fiber is simpler to fabricate than adding more cladding rings.

To get a better understanding of this redistribution of energy density due to the modified or missing corner strands, we plot in Fig. 4 the real part of S_ρ at the wavelengths of minimum loss in the first bandgap for the photonic bandgap fiber with $R = 0$ (a), $R = r$ (b), and $R \approx 1.5r$ (c) in four directions, from the center of the fiber (indicated by different colors and linestyles in the schematic of the fibers). It is seen that there is backscattering of light, indicated by the negative values of S_ρ, back into the core for the case of $R = 0$ (a) and $R \approx 1.5r$ (c), which leads to the redistribution of energy density towards the core region, while light passes through the fiber

Optics EXPRESS

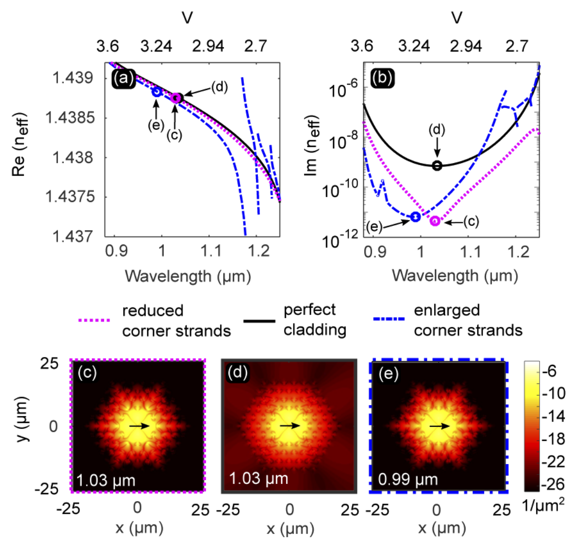

Fig. 3. Results equivalent to Fig. 2 for the second bandgap for structures having $R = r$ (black solid lines), $R \approx 0.35r$ (magenta dotted lines) and $R \approx 1.45r$ (blue dashed-dotted lines). In contrast to the first bandgap, the best confinement is achieved for the structure with modified corner strands for $R \approx 0.35r$.

without any backscattering for the unmodified cladding with $R = r$ (b). We also see that the scale of Fig. 4(a) is an order of magnitude lower, which corresponds to a lower leakage of energy in the radial direction compared to the other two structures. We plot in Figs. 4(d)-(f) the real part of S_ρ at a position corresponding to the center of the first inclusion in each direction for the structures with (d) missing, (e) enlarged, and (f) unmodified corner strands. Note that there is no rod in the corner directions for the missing (d) corner strand structure. The wavelength of minimum loss is indicated by the vertical line for their respective structures. Im(n_{eff}) is also plotted as a function of wavelength in (d-f). It is seen that for the missing (d) and enlarged (f) corner strands, the backscattering occurs at different rods as we sweep across the wavelength, and the interchange in backscattering of the rods occurs close to the wavelength of the minimum loss of the structure [Fig. 4(d) and (f)], while no backscattering is observed for the unmodified structure [Fig. 4(e)]. For the modified structures, the lowest loss occurs when there is optimal backscattering from all rods in the core surround, while this mechanism of backscattering is absent in the case of the unmodified structure.

The real part of S_ρ for the second bandgap is displayed in Fig. 5 for the three structures with reduced, unmodified, and enlarged corner strands. We can see that the radial energy density is two orders of magnitude lower for the structures with modified corner strands [Fig. 5(a) and (c)] than for unmodified corner strands [Fig. 5(b)], indicating lower leakage of energy to the homogeneous background. We also observe that backscattering into the fiber core takes place for the reduced-corner-strand structure in just one dominant direction compared to the enlarged-corner-strand structure at the wavelength of lowest loss. The spectral distribution of the real part of S_ρ and Im(n_{eff}) is displayed for the second bandgap in Fig. 5(d)-(f) at the same positions as described in Fig. 4(d)-(f). We can see that there is no backscattering for the unmodified (e) cladding, while an interchange in the direction of backscattering occurs for the structures with modified corner strands (d,f), near the wavelength of lowest loss, as observed in the first bandgap as well.

In Fig. 6, we plot the dependence of loss on the V parameter and the ratio of corner strand radii R over strand radius r for two different ratios of r/Λ for the first and second bandgap. For

Optics EXPRESS

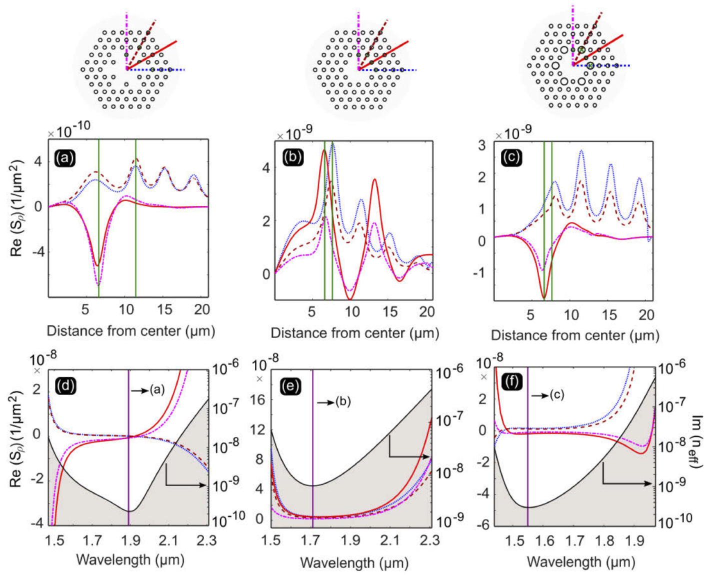

Fig. 4. Real value of the time-averaged Poynting vector in the radial direction for the x-polarized fundamental mode in the first bandgap, with missing corner strands at λ = 1.89 µm (a), unmodified cladding at λ = 1.71 µm (b) and with enlarged corner strands (R = 1.16 µm) at λ = 1.55 µm (c). All other parameters are the same as in Fig. 2. The selected wavelengths correspond to the minimum loss of the respective structures. The fields are plotted in four different transverse directions from the center as shown in the insets. The vertical lines in (a-c) mark the position of the center of the first inclusion in each direction. The bottom panels display the spectral distribution of the real part of the radial Poynting vector component at the center of the rods along these directions for missing (d), without (e), and with (f) enlarged corner strands. The gray curve indicates Im(n_{eff}) of the respective structures (right axis). For the sake of comparability, the field distributions have been normalized analytically using Eq. (2). The vertical lines in (d-f) mark the wavelength of lowest loss. It can be seen in (a) and (c), that backscattering of light to the core occurs in the presence of the enlarged and missing-corner-strand structures, resulting in a decrease of the fiber loss.

r/Λ = 0.2, low loss is observed around missing corner strands as well as enlarged corner strands in the first bandgap, see Fig. 6(a), as expected from previous results for the same structure. For the higher r/Λ ratio of 0.3, it can be seen that the structure with missing corner strands no longer exhibits the lowest loss. The lowest loss is observed for the structure with modified corner strands with a smaller corner strand radii than in the ideal structure. In the second bandgap, we also observe that missing corner strands do not provide the lowest loss for both ratios of radius-to-pitch, see Fig. 6(b) and (d), while modifying the corner strands by either reducing or increasing the strand radius provides low loss. However, we see that the region of low loss for the enlarged corner strands is much broader than the region of low loss from reducing the corner strands, while the difference between losses for enlarged and reduced corner strands is very low. Therefore, enlarging the corner strands will be less sensitive with respect to fabrication inaccuracies. Note the occurrence of little peaks, which arise close to discontinuities in Fig. 6(a)-(d) due to switching from one hybrid mode to another at anticrossings. Also, one can notice that the loss reduction is higher for the lower ratio of r/Λ. Further simulations with different ratios of r/Λ confirm this trend (not shown here). Nevertheless, our approach allows for reducing the loss independently of the ratio of r/Λ.

Optics EXPRESS

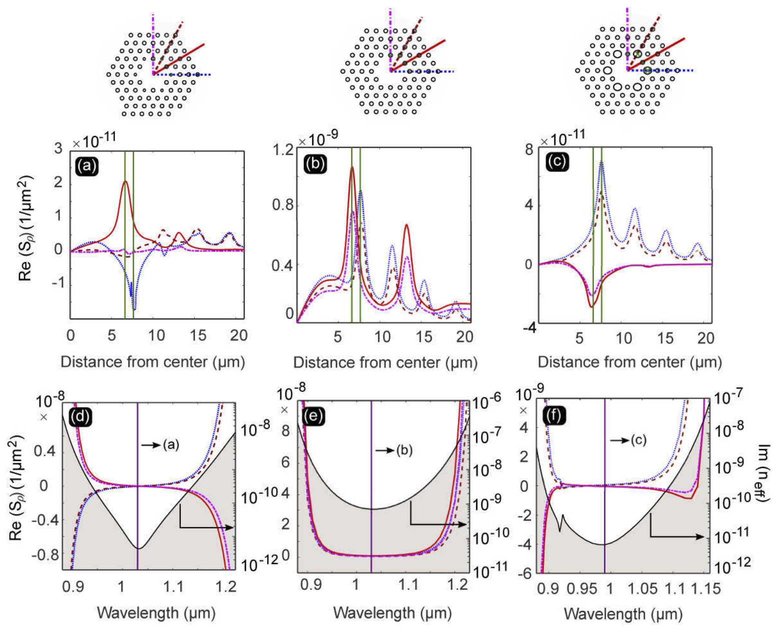

Fig. 5. Results equivalent to Fig. 4, but for the second bandgap, with reduced corner strands (R = 0.27 μm) at λ = 1.03 μm (a), unmodified cladding at λ = 1.03 μm (b), and with enlarged corner strands (R = 1.11 μm) at λ = 0.99 μm (c). It can be seen that backscattering of light to the core occurs for the second bandgap only in the presence of the modified corner strands. The vertical lines in (d-f) mark the wavelengths of lowest loss.

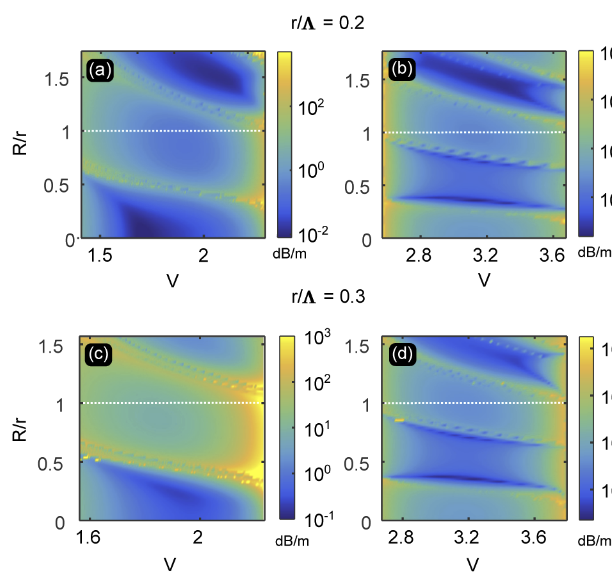

Fig. 6. Loss as a function of V parameter and the ratio between corner strand radius R and strand radius r in the first (a,c) and second (b,d) bandgap for r/Λ = 0.2(a, b) and r/Λ = 0.3 (c, d). Evidently, the ideal choice of corner strand radius significantly depends on the bandgap and the ratio of strand radius and Λ.

Optics EXPRESS

For all cases, we infer that the subtle interplay of backscattering by small and large strand radii in the core surround leads to a lower loss compared to the unmodified structure. In general, varying the corner strand radius turns out to be a versatile method for reducing the losses without increasing the complexity during the fabrication process significantly for the considered geometries. The trade-off in some cases maybe the presence of a higher number of cladding supermodes for a given strand radius, which has a significant impact on the dispersion.

Futhermore, we show in Fig. 7 that the low loss behavior is tolerant towards fabricational imperfections such as position and diameter deviations. In order to simulate these imperfections, the diameter and position of all the strands in the cladding are varied within a specific range. To demonstrate the low-loss behavior, the same realization of disorder is studied with enlarged corner strands of the optimal radius (R = 1.16 μm). The calculations are then repeated for 50 realizations of disorder. It is clear from Fig. 7 that for the considered amount of disorder, where each inclusion is shifted by maximum 0.2 μm for position disorder or changed by 2% in size for diameter disorder, the low loss behavior prevails.

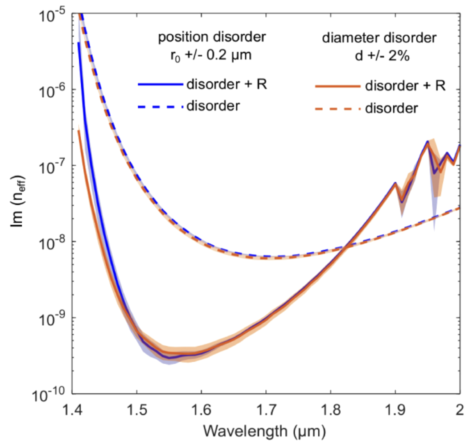

Fig. 7. Imaginary part of the effective index as a function of wavelength for postion disorder (blue) with and without enlarged corner strands (solid and dashed lines, respectively) and diameter disorder (orange) with and without enlarged corner strands (solid and dashed lines, respectively). The shaded region represents the standard deviation calculated using 50 realizations of disorder for each case. It can be seen that for the considered amount of disorder, where each inclusion is shifted by maximum 0.2 μm for position disorder or changed by 2% in size for diameter disorder, the low loss behavior with enlarged corner strands perseveres.

3. Conclusion

In summary, we have presented a novel pathway to reduce the losses in photonic bandgap fibers by introducing symmetrically modified corner strands in the core surround. We demonstrate the behavior of the fundamental core mode for different corner strand radii and obtain ideal corner strand radii for the lowest attenuation, while the actual value of the loss is reduced by more than two orders of magnitude. We show this for both the first and second bandgaps. We demonstrate that this low loss behavior prevails even in the presence of fabricational disorders such as position and diameter disorder. We also observe that the introduction of the modified strands narrows the effective bandgap, for certain modified strand radii of the structure due to the presence of cladding supermodes, which imposes anticrossings of strand and fundamental core modes. Our approach can principally be used for reducing the confinement loss in all kinds of photonic bandgap fibers

Optics EXPRESS

including hollow-core or all-solid photonic bandgap fibers. Our simulations show that the crucial quantity is the V parameter, implying that either the strand diameter or their refractive index may be modified.

Funding. Deutsche Forschungsgemeinschaft (SCHM2655/11-1, SCHM2655/15-1, SCHM2655/8-1, SPP 1839).

Disclosures. The authors declare no conflicts of interest.

References

1. P. Russell, "Photonic crystal fibers," Science **299**(5605), 358–362 (2003).
2. A. M. Cubillas, S. Unterkofler, T. G. Euser, B. J. Etzold, A. C. Jones, P. J. Sadler, P. Wasserscheid, and P. S. J. Russell, "Photonic crystal fibres for chemical sensing and photochemistry," Chem. Soc. Rev. **42**(22), 8629–8648 (2013).
3. G. Li, M. Zeisberger, and M. A. Schmidt, "Guiding light in a water core all-solid cladding photonic band gap fiber–an innovative platmu for fiber-based optofluidics," Opt. Express **25**(19), 22467–22479 (2017).
4. P. S. J. Russell, P. Hölzer, W. Chang, A. Abdolvand, and J. Travers, "Hollow-core photonic crystal fibres for gas-based nonlinear optics," Nat. Photonics **8**(4), 278–286 (2014).
5. J. C. Travers, W. Chang, J. Nold, N. Y. Joly, and P. S. J. Russell, "Ultrafast nonlinear optics in gas-filled hollow-core photonic crystal fibers," J. Opt. Soc. Am. B **28**(12), A11–A26 (2011).
6. A. B. Fedotov, A. N. Naumov, A. M. Zheltikov, I. Bugar, D. Chorvat, A. P. Tarasevitch, and D. von der Linde, "Frequency-tunable supercontinuum generation in photonic-crystal fibers by femtosecond pulses of an optical parametric amplifier," J. Opt. Soc. Am. B **19**(9), 2156–2164 (2002).
7. G. Epple, K. Kleinbach, T. G. Euser, N. Joly, T. Pfau, P. S. J. Russell, and R. Löw, "Rydberg atoms in hollow-core photonic crystal fibres," Nat. Commun. **5**(1), 4132 (2014).
8. F. Poletti, N. Wheeler, M. Petrovich, N. Baddela, E. N. Fokoua, J. Hayes, D. Gray, Z. Li, R. Slavík, and D. Richardson, "Towards high-capacity fibre-optic communications at the speed of light in vacuum," Nat. Photonics **7**(4), 279–284 (2013).
9. F. Benabid and P. Roberts, "Linear and nonlinear optical properties of hollow core photonic crystal fiber," J. Mod. Opt. **58**(2), 87–124 (2011).
10. S. Hanf, R. Keiner, D. Yan, J. Popp, and T. Frosch, "Fiber-enhanced Raman multigas spectroscopy: a versatile tool for environmental gas sensing and breath analysis," Anal. Chem. **86**(11), 5278–5285 (2014).
11. C. Jain, A. Braun, J. Gargiulo, B. Jang, G. Li, H. Lehmann, S. A. Maier, and M. A. Schmidt, "Hollow core light cage: Trapping light behind bars," ACS Photonics **6**(3), 649–658 (2019).
12. B. Jang, J. Gargiulo, R. F. Ando, A. Lauri, S. A. Maier, and M. A. Schmidt, "Light guidance in photonic band gap guiding dual-ring light cages implemented by direct laser writing," Opt. Lett. **44**(16), 4016–4019 (2019).
13. E. N. Fokoua, F. Poletti, and D. J. Richardson, "Analysis of light scattering from surface roughness in hollow-core photonic bandgap fibers," Opt. Express **20**(19), 20980–20991 (2012).
14. P. Roberts, F. Couny, H. Sabert, B. Mangan, D. Williams, L. Farr, M. Mason, A. Tomlinson, T. Birks, J. Knight, and P. St. J. Russell, "Ultimate low loss of hollow-core photonic crystal fibres," Opt. Express **13**(1), 236–244 (2005).
15. J. Broeng, D. Mogilevstev, S. E. Barkou, and A. Bjarklev, "Photonic crystal fibers: A new class of optical waveguides," Opt. Fiber Technol. **5**(3), 305–330 (1999).
16. G. Ren, P. Shum, L. Zhang, X. Yu, W. Tong, and J. Luo, "Low-loss all-solid photonic bandgap fiber," Opt. Lett. **32**(9), 1023–1025 (2007).
17. W. Tong, H. Wei, J. Li, H. Wang, Q. Han, J. Luo, G. Ren, X. Yu, and P. Shum, "Investigation of all-solid photonic bandgap fiber with low losses in low-order bandgaps," Opt. Quantum Electron. **39**(12-13), 1071–1080 (2007).
18. J.-H. Liu and C.-P. Yu, "Loss-reduced internally liquid-filled photonic crystal fibers," in *Photonic and Phononic Crystal Materials and Devices X*, vol. 7609 (International Society for Optics and Photonics, 2010), p. 76091M.
19. Q. Fang, Z. Wang, L. Jin, J. Liu, Y. Yue, Y. Liu, G. Kai, S. Yuan, and X. Dong, "Dispersion design of all-solid photonic bandgap fiber," J. Opt. Soc. Am. B **24**(11), 2899–2905 (2007).
20. M. Pourmahayabadi and S. M. Nejad, "Optimal confinement loss reduction in photonic crystal fiber with flattened dispersion," in *High Capacity Optical Networks and Enabling Technologies, 2008. HONET 2008. International Symposium*, (IEEE, 2008), pp. 265–270.
21. E. N. Fokoua, D. J. Richardson, and F. Poletti, "Impact of structural distortions on the performance of hollow-core photonic bandgap fibers," Opt. Express **22**(3), 2735–2744 (2014).
22. T. Yang, C. Ding, R. W. Ziolkowski, and Y. J. Guo, "A scalable THz photonic crystal fiber with partially-slotted core that exhibits improved birefringence and reduced loss," J. Lightwave Technol. **36**(16), 3408–3417 (2018).
23. P. Roberts, D. Williams, B. Mangan, H. Sabert, F. Couny, W. Wadsworth, T. Birks, J. Knight, and P. S. J. Russell, "Realizing low loss air core photonic crystal fibers by exploiting an antiresonant core surround," Opt. Express **13**(20), 8277–8285 (2005).
24. H. K. Kim, J. Shin, S. Fan, M. J. Digonnet, and G. S. Kino, "Designing air-core photonic-bandgap fibers free of surface modes," IEEE J. Quantum Electron. **40**(5), 551–556 (2004).
25. P. Steinvurzel, C. M. de Sterke, M. Steel, B. Kuhlmey, and B. Eggleton, "Single scatterer Fano resonances in solid core photonic band gap fibers," Opt. Express **14**(19), 8797–8811 (2006).
26. F. Poletti, N. G. Broderick, D. J. Richardson, and T. M. Monro, "The effect of core asymmetries on the polarization properties of hollow core photonic bandgap fibers," Opt. Express **13**(22), 9115–9124 (2005).

Optics EXPRESS

27. C. M. Smith, N. Venkataraman, M. T. Gallagher, D. Müller, J. A. West, N. F. Borrelli, D. C. Allan, and K. W. Koch, "Low-loss hollow-core silica/air photonic bandgap fibre," Nature **424**(6949), 657–659 (2003).
28. R. Amezcua-Correa, F. Gérôme, S. G. Leon-Saval, N. Broderick, T. A. Birks, and J. C. Knight, "Control of surface modes in low loss hollow-core photonic bandgap fibers," Opt. Express **16**(2), 1142–1149 (2008).
29. M. Petrovich, N. Baddela, N. Wheeler, E. Numkam, R. Slavik, D. R. Gray, J. R. Hayes, J. Wooler, F. Poletti, and D. J. Richardson, "Development of low loss, wide bandwidth hollow core photonic bandgap fibers," in *Optical Fiber Communication Conference and Exposition and the National Fiber Optic Engineers Conference (OFC/NFOEC), 2013* (IEEE, 2013), pp. 1–3.
30. S. Upendar, I. Allayarov, M. Schmidt, and T. Weiss, "Analytical mode normalization and resonant state expansion for bound and leaky modes in optical fibers-an efficient tool to model transverse disorder," Opt. Express **26**(17), 22536–22546 (2018).
31. I. Allayarov, S. Upendar, M. Schmidt, and T. Weiss, "Analytic mode normalization for the Kerr nonlinearity parameter: Prediction of nonlinear gain for leaky modes," Phys. Rev. Lett. **121**(21), 213905 (2018).
32. M. Chemnitz, M. Gebhardt, C. Gaida, F. Stutzki, J. Kobelke, J. Limpert, A. Tünnermann, and M. A. Schmidt, "Hybrid soliton dynamics in liquid-core fibres," Nat. Commun. **8**(1), 42 (2017).
33. J. Fleming, "Material and mode dispersion in GeO2· B2O3· SiC2 glasses," J. Am. Ceram. Soc. **59**(11-12), 503–507 (1976).
34. T. White, B. Kuhlmey, R. McPhedran, D. Maystre, G. Renversez, C. M. De Sterke, and L. Botten, "Multipole method for microstructured optical fibers. I. Formulation," J. Opt. Soc. Am. B **19**(10), 2322–2330 (2002).
35. B. T. Kuhlmey, T. P. White, G. Renversez, D. Maystre, L. C. Botten, C. M. de Sterke, and R. C. McPhedran, "Multipole method for microstructured optical fibers. II. Implementation and results," J. Opt. Soc. Am. B **19**(10), 2331–2340 (2002).
36. A. Argyros, T. Birks, S. Leon-Saval, C. Cordeiro, and P. S. J. Russell, "Guidance properties of low-contrast photonic bandgap fibres," Opt. Express **13**(7), 2503–2511 (2005).
37. I. Allayarov, A. Schmidt, and T. Weiss, "Theory of four-wave mixing for bound and leaky modes," Phys. Rev. A **101**, 043806 (2020).